Environmental Science: Atmospheres

ROYAL SOCIETY OF CHEMISTRY

PAPER

View Article Online
View Journal | View Issue

Cite this: *Environ. Sci.: Atmos.*, 2025, **5**, 1110

Size-resolved cloud droplet acidity over the US

Stylianos Kakavas, [a] Georgios Siderakis[b] and Spyros N. Pandis *[ab]

The acidity of cloud droplets can vary with size due to differences in aerosol composition and cloud chemistry and differential soluble gas uptake. Chemical transport models (CTMs) often assume that all droplets have the same composition and therefore acidity. In this work, we use the PMCAMx CTM to simulate size-resolved cloud and fog droplet acidity over the US during a winter and a summer month as a function of altitude. Small droplets are assumed to form on the activated particles smaller than 2.5 μm and have an average diameter of 20 μm, whereas large droplets form on the coarse particles and have an average diameter of 30 μm. Our simulations show that large droplets are often more alkaline than small (up to 100% lower H^+ concentrations) especially in regions influenced by dust. In areas with more acidic conditions, the difference in H^+ concentrations between small and large droplets is smaller. The pH of droplets either decreases or increases with altitude, depending on the composition of the aerosol on which the droplets were formed. Comparison of the bulk and two-section size-resolved approaches indicates that current differences in aqueous-phase sulfate concentrations over the US are generally low and usually less than 20% at approximately 10 min intervals (the most frequent difference ranges from zero to 5%). Based on our results, bulk calculations can simulate current aerosol composition and droplet pH over the US with small discrepancies. This is due to reduced SO_2 emissions causing SO_2 levels in clouds to often fall below those of H_2O_2. Under these conditions the importance of the pH-dependent ozone sulfate production pathway is diminished. These findings are specific to the US and may not apply to regions with higher SO_2 emissions.

Received 9th June 2025
Accepted 2nd September 2025

DOI: 10.1039/d5ea00067j

rsc.li/esatmospheres

Environmental significance

This study investigates the variability of the acidity of clouds over a continental region (US) as a function of season, altitude and droplet size. Clouds and fogs are important for many atmospheric processes, affecting air quality and climate. One of the most significant properties of these droplets is their acidity which determines the partitioning of acids and bases between the gas and aqueous phases, the rates of reactions, and their corresponding wet removal rates. Cloud evaporation leads to aerosol formation, and therefore aerosol composition and acidity can be directly affected by aqueous-phase chemistry.

1. Introduction

Clouds and fogs are important for many atmospheric processes, affecting air quality and climate.[1] One of the most significant properties of these droplets is their acidity which determines the partitioning of acids and bases between the gas and aqueous phases, the rates of reactions, and their corresponding wet removal rates.[2,3] Cloud evaporation leads to aerosol formation, and therefore aerosol composition and acidity can be directly affected by aqueous-phase chemistry.[2]

The calculation of cloud droplet pH has long been a part of chemical transport and climate models because of the need to simulate sulfate production. Sulfate is an important component of fine particulate matter, and its production in cloud and fog droplets is significantly influenced by droplet acidity.[4] Many chemical transport and climate models, such as CAM-Chem, CMAQ, GEOS-Chem, TM4-ECPL, and WRF-Chem incorporate cloud water pH in their calculations.[2] In some of these models the calculation of cloud pH is simplified. For example, CAM-Chem does not account for particulate nitrate, and it does not explicitly account for the oxidation of S(IV) by ozone and hydrogen peroxide.[2,5] Other models, such as TM4-ECPL and GEOS-Chem, neglect the effects of dust.[6–9] In some model applications a constant droplet pH is assumed.[10,11] Measurements of cloud droplet pH have shown that small droplets are often more acidic than the larger ones, indicating a pH dependence on droplet size.[12] Most models use bulk droplet pH neglecting the heterogeneity of cloud droplets. Previous studies have shown that the bulk droplet approach can underestimate sulfate production rates from aqueous-phase chemistry.[1,13–15] Shah *et al.* (2020)[16] improved GEOS-Chem cloud water pH predictions by including the effects of carboxylic acids and dust, but they did not account for droplet size. Fahey and Pandis

[a]*Institute of Chemical Engineering Sciences (ICE-HT/FORTH), Patras, GR 26504, Greece*

[b]*Department of Chemical Engineering, University of Patras, Patras, GR 26504, Greece. E-mail: spyros@chemeng.upatras.gr*

(2001)[13] developed a computationally efficient size-resolved aqueous-phase chemistry module (Variable Size Resolution Model or VSRM), which simulates the mass transfer between the gas phase and different groups of droplets. This model in its default operation mode determines whether bulk or two-section size-resolved chemistry should be applied based on a set of semi-empirical rules. The size-dependence of cloud drop composition can also impact other atmospheric processes, such as wet removal rates of pollutants, ice formation, *etc.*

Despite the above progress, there are still large discrepancies in droplet pH predictions among chemical transport and climate models, especially in areas influenced by dust.[2] Also, measurements of cloud and fog droplet pH indicate that there can be significant errors in the simulated pH.

In this study, we use the PMCAMx chemical transport model (CTM), which incorporates VSRM, to simulate the size-resolved acidity of cloud and fog droplets over the US for a wintertime and a summertime period (February and July 2017). Our objective is to quantify the pH variation between small and large droplets and its dependence on location and altitude. We also present results based on the bulk droplet assumption, examining its impact on particle composition, and compare our predictions with cloud water pH measurements from specific locations.

2. Model description

2.1 PMCAMx

The PMCAMx CTM used in this work is the research version of the CAMx model.[17] The gas-phase chemical mechanism used is a modified version of SAPRC,[18] and includes 237 reactions of 91 gas species and 18 radicals. To describe the aerosol size and composition distribution, a 10-size section representation (diameters from 40 nm to 40 μm) is used, assuming that each size bin is internally mixed. Therefore, PMCAMx can predict PM_x concentrations where x can be equal to (among other choices) 1, 2.5, and 10 μm. The aerosol components considered in the model include sulfate, nitrate, ammonium, sodium, chloride, potassium, calcium, magnesium, other inert crustal species, elemental carbon, primary and secondary organic species and water. The aerosol and gas phases are assumed to be always in equilibrium in the present study, while for the thermodynamic calculations of inorganic aerosol species the ISORROPIA-lite model is used, which assumes that aerosol is always in metastable state (liquid aerosol) even at low RH.[19] ISORROPIA-lite also considers the effects of secondary organic aerosol (SOA) water on inorganic aerosol thermodynamics. In this work, the SOA hygroscopicity parameter is assumed to be equal to 0.15.[19,20] For the simulation of primary and secondary organic aerosols, the volatility basis set (VBS) approach of Donahue *et al.* (2006)[21] is used, while aqueous-phase chemistry is simulated using the VSRM module of Fahey and Pandis (2001)[13] as described below.

2.2 VSRM

The Variable Size Resolution Model (VSRM) is based on the chemical mechanism of Pandis and Seinfeld (1989),[22] but includes Ca^{2+} in the list of particle components as well as H_2SO_4 in the gas phase. In this work, K^+ and Mg^{2+} have been added to the list of simulated particle components together with their impact on the acidity of droplets through the ion balance. VSRM simulates the evolution of 21 gas-phase and 50 aqueous-phase species and includes 109 aqueous-phase chemical reactions. It calculates the time-dependent uptake of gases into droplets separately for each droplet group by solving the corresponding differential equations, as described by Fahey and Pandis (2001).[13] VSRM was originally developed to save computational time in aqueous-phase chemistry simulations due to its capability to perform either bulk or two-section calculations depending on the composition. Fahey and Pandis (2001)[13] have shown that this approach allows sulfate predictions to match closely the predictions of a six-section size-resolved model, while reducing the computational cost by an order of magnitude.

Droplets are assumed to be formed instantaneously on particles with size above a critical dry diameter, with smaller particles assumed to be interstitial aerosol. Fahey and Pandis (2001)[13] originally assumed a critical diameter of 0.7 μm. However, more recent studies suggest a lower average critical diameter.[23,24] In this study, we assume a critical diameter of 0.3 μm. Therefore, particles in the first three size bins of PMCAMx are considered interstitial aerosol. Particles with dry diameters larger than the critical diameter and up to 2.5 μm become "small" droplets, while particles with dry diameters greater than 2.5 μm become "large" droplets. The 2.5 μm cutoff is an empirical choice used to separate more acidic ($PM_{2.5}$) from alkaline ($PM_{2.5-10}$) particles, based on findings from previous studies on aerosol acidity. A 1 μm cutoff could also be considered as an alternative. Small droplets are assumed to have an average diameter of 20 μm, while large droplets have an average diameter of 30 μm. For bulk calculations, an average droplet diameter of 20 μm is assumed. It should be noted that sulfate predictions are not significantly affected by the assumed droplet diameters.[14]

Gas phase concentrations, cloud liquid water content (LWC), and aerosol size and composition distribution are the main inputs to the aqueous-phase module. VSRM is applied in PMCAMx when LWC and temperature are higher than 0.05 g m^{-3} and 268 K in a grid cell respectively, as it handles liquid cloud microphysics exclusively. At lower temperatures, ice processes, which VSRM does not support, dominate. Also, it is assumed that 80% of the cloud's liquid water is in the form of small droplets while the remaining 20% in the large droplets. The 80 : 20 split between small and large drops is an empirical choice based on measurements showing that large drops initially constitute a small fraction of the total LWC and grow through coalescence.[4] Droplet pH is calculated by VSRM for each grid cell at time steps ranging from 7 to 24 min when clouds or fog are present. More details about VSRM can be found in Fahey and Pandis (2001; 2003).[13,14]

3. Model application

PMCAMx was used to simulate size-resolved cloud and fog droplet acidity over the US during February and July 2017. The

modeling domain covers an area of 4752 × 2952 km^2, which includes northern Mexico and southern Canada. The horizontal grid resolution is 36 × 36 km, while the vertical domain consists of 14 layers extending up to 6 km in altitude.

For meteorological inputs to PMCAMx, the Weather Research and Forecasting (WRF v3.6.1) model was used, with a horizontal resolution of 12 km across the entire domain. Emission data for the simulations were based on the 2017 National Emissions Inventory.[25] Wind-blown dust emissions were simulated using the WBDUST model, which is provided by Ramboll as a pre-processing tool for CAMx (**https://www.camx.com/download/support-software**). In this study, calcium, potassium, magnesium, and sodium represented 2.4%, 1.5%, 0.9%, and 1.2% of the emitted dust respectively.[26] More details about the WBDUST model can be found in Liaskoni *et al.* (2023).[27] A detailed description of WBDUST application can be found in Kakavas *et al.* (2025).[28] The PMCAMx predictions in terms of aerosol levels and composition for the simulated periods were found satisfactory by Kakavas *et al.* (2025).[28] More specifically, the model's performance ranged from good to average for daily concentrations of total $PM_{2.5}$, total PM_{coarse}, and the individual components of $PM_{2.5}$ based on the criteria of Morris *et al.* (2005).[29]

Two PMCAMx simulations were performed for both February and July 2017. In the first simulation, two-section size-resolved chemistry calculations were performed by VSRM, and a comparison between small and large droplets acidity is presented. A second simulation was performed assuming that all droplets had the same size (bulk approach). The inputs for both simulations were identical.

4. Results

4.1 Cloud and fog presence time

For both periods, there are cloud and fog free areas, as well as regions with high fog and cloud presence (up to 60% of the total simulated time). The average predicted presence time of clouds and fogs for each PMCAMx vertical layer for both simulated periods is presented in Fig. S1 and S2 (SI), respectively. Higher cloud presence is predicted for both simulated periods in the eastern part of the US and the areas covered by sea (parts of the Atlantic and Pacific oceans). The average cloud LWC is, as expected, higher in these regions (Fig. S3 and S4, SI). In the western US, the predicted presence of clouds and fogs is lower (up to 10% of the simulated time), but there are also areas (*e.g.*, parts of California during wintertime and Colorado during summertime) with higher cloud and fog presence frequency (up to 50%). The frequency of cloud and fog presence is an important factor for ensuring that droplet pH predictions are representative of each area.

4.2 Altitude, seasonal and size dependence of droplet pH

During wintertime, the predicted pH of both droplet sizes ranges from 2.5 to 8 across the US, with the relative frequency of pH predictions varying depending on altitude and location (Fig. 1). The average predicted pH is 4.9 ± 1.0 for small droplets and 5.1 ± 1.2 for large droplets. The average predicted pH of small and large droplets over the US at altitudes between 640 and 980 m is shown in Fig. 2. Results for other altitude ranges are shown in Fig. S5 and S6 (SI). For both droplet sizes, higher pH values are predicted in the western part of the US due to the higher concentrations of alkaline dust.[28] In the eastern part, the higher concentrations of acidic particle components like sulfate combined with the higher concentrations of acidic gases (*e.g.*, HNO_3), lead to lower droplet pH predictions. Cloud water acidity is often compared to the CO_2–H_2O system, which has a pH of 5.5 at current CO_2 levels.[16] Lower pH values are considered acidic, while higher alkaline. At altitudes up to 300 m, the most frequent pH prediction is between 3 and 4 for small droplets and between 4 and 5 for large droplets (Fig. 1). However, as altitude increases, the pH distribution becomes narrower with most values in the 4–6 range. Particles and gases concentrations decrease with altitude leading to a change in cloud pH. For example, in the western US, where dust concentrations are higher, its decrease with altitude leads to lower

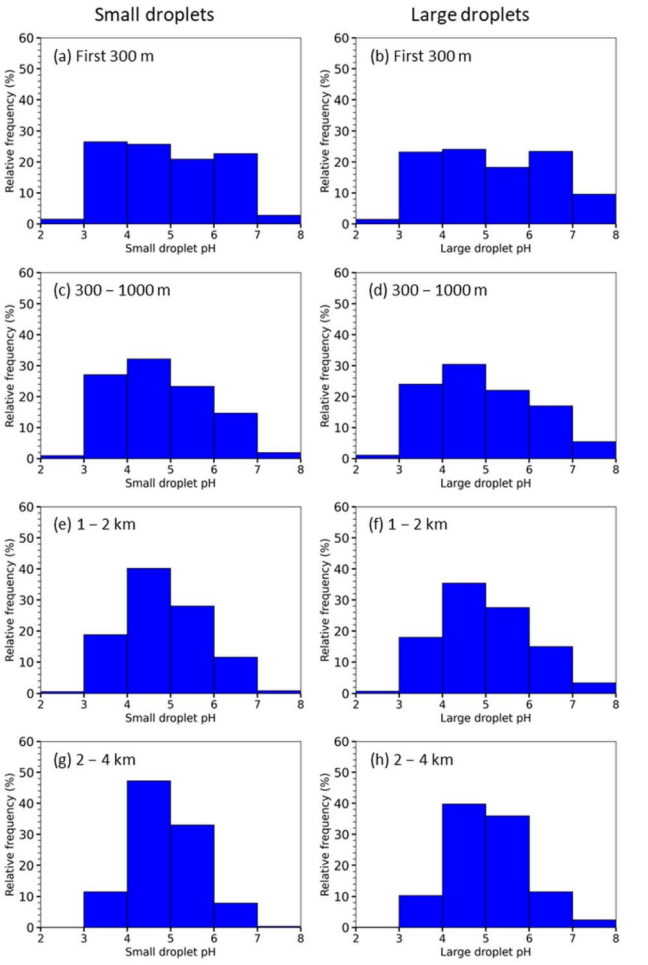

Fig. 1 Frequency distributions of pH predictions at 10 min intervals for small and large droplets over the US during February 2017 at different altitudes: (a) and (b) first 300 m, (c) and (d) 300–1000 m, (e) and (f) 1000–2000 m, (g) and (h) 2000–4000 m.

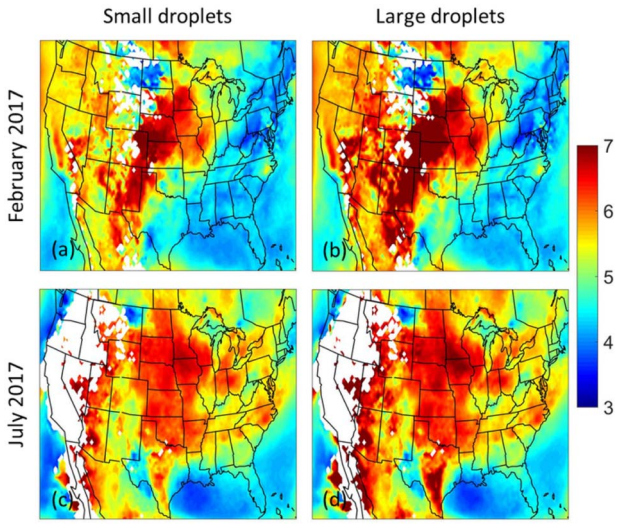

Fig. 2 Average predicted pH of small and large droplets at altitudes between 640 and 980 m during: (a) and (b) February 2017, (c) and (d) July 2017. The white colour corresponds to cloud and fog free areas.

average droplet pH at higher altitudes (Fig. 3). Concentrations of acidic components also decrease with altitude in the western US, but those of basic components decrease at higher rates (Fig. S7, SI). In contrast, in the eastern US, where acidic components are prevalent, their decrease with altitude leads to higher average droplet pH at higher altitudes (Fig. 3). Partially responsible for this change is also the increase of cloud LWC with altitude (Fig. S8, SI).

During summertime, higher droplet pH values are predicted more frequently compared to wintertime (Fig. 4), with average pH values of 5.1 ± 0.9 for small droplets and 5.3 ± 1.0 for large droplets. At altitudes up to 300 m, the most frequent pH prediction for both droplet sizes is between 5 and 6 units. However, as altitude increases, the pH distribution becomes narrower with most values in the 4–6 range just like wintertime. Summer droplet pH is higher in the eastern part of the US compared to wintertime period with differences up to 2 units (Fig. 2). Results for other altitude ranges are also shown in Fig. S9 and S10 (SI). In the western part, higher pH values are predicted compared to the East. The higher concentrations of alkaline dust and ammonia during summertime over the US lead to higher pH predictions for both droplet sizes. In the western US, average droplet pH decreases with altitude, whereas in the eastern US, it increases with altitude (Fig. 3). For both simulated periods, higher droplet pH is predicted over the Great Plains and Midwest, where high NH_3 emissions strongly influence cloud water pH. Future pH increases may also result from rising wildfire emissions and warmer soil temperatures in these regions.

In general, large droplets have lower H^+ concentrations over the US (up to *a* factor of 2) compared to small droplets. The

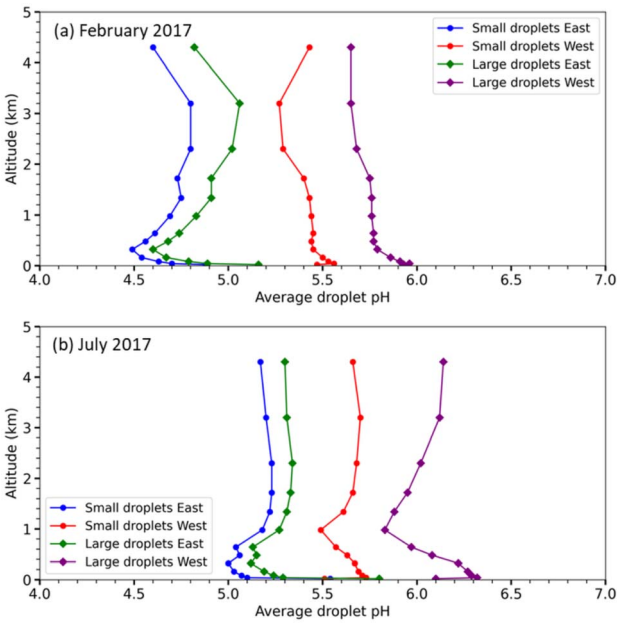

Fig. 3 Average predicted pH of small and large droplets as a function of altitude for the eastern and western US during: (a) February 2017, and (b) July 2017.

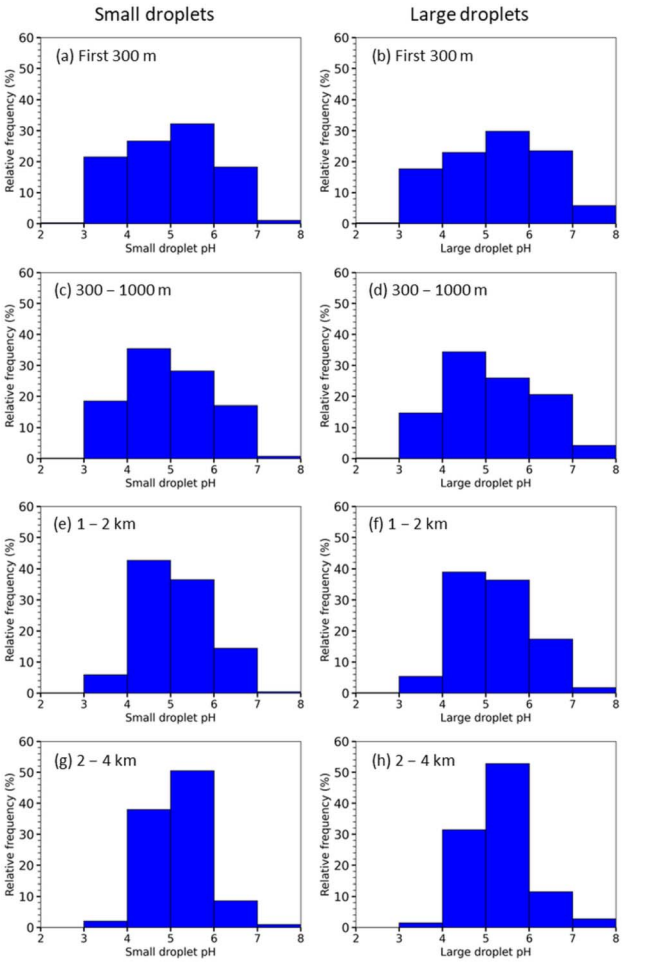

Fig. 4 Frequency distributions of pH predictions at 10 min intervals for small and large droplets over the US during July 2017 at different altitudes: (a) and (b) first 300 m, (c) and (d) 300–1000 m, (e) and (f) 1000–2000 m, (g) and (h) 2000–4000 m.

frequency distributions of the fractional difference in H^+ concentrations between large and small droplets over the US during both simulated periods are shown in Fig. 5. A negative fractional difference indicates that large droplets have lower H^+ concentrations than small droplets. At altitudes up to 300 m, the most frequent fractional difference in H^+ concentrations between large and small droplets is −40 to −20% during wintertime and −60 to −40% during summertime. As altitude increases, the most frequent fractional difference in H^+ concentrations ranges from −40% to −20% during wintertime and from −20% to 0% during summertime. The variation in H^+ concentrations between small and large droplets is due to differences in cloud chemistry related to droplet size,[30] the lower condensational rates of acid gases in large droplets (lower surface area-to-volume ratio) and the greater volume of water in large droplets which dilutes acids more effectively.[12,31] However, there are some cases (10–20% of predictions) in both simulated periods where small droplets have slightly lower H^+ concentrations than large droplets (usually up to 20%). This is primarily due to the higher surface area-to-volume ratio of small droplets, which enhances their ability to absorb NH_3 when this base dominates the system. Hu *et al.* (2019)[15] have also shown that the H^+ concentration of large droplets can be higher compared to small during the initial stage of cloud formation.

The higher pH differences between small and large droplets are predicted in areas with higher dust concentrations (such as the western US) for both simulated periods (Fig. 6). Results for other altitude ranges are shown in Fig. S11 and S12 (SI). In contrast, in the eastern US, higher concentrations of acidic particles and gases, which can dissolve in droplet water, lead to lower pH values for both droplet sizes. As a result, lower pH differences are predicted between small and large droplets in these areas (Fig. 6). Additionally, as altitude increases, the reduction in particle and gas concentrations leads to a corresponding change in droplet pH. This change can either be a decrease or an increase, depending on whether the particles and gases contribute acidic or basic substances to the cloud water. Another factor influencing this change is the increase in cloud LWC with altitude.

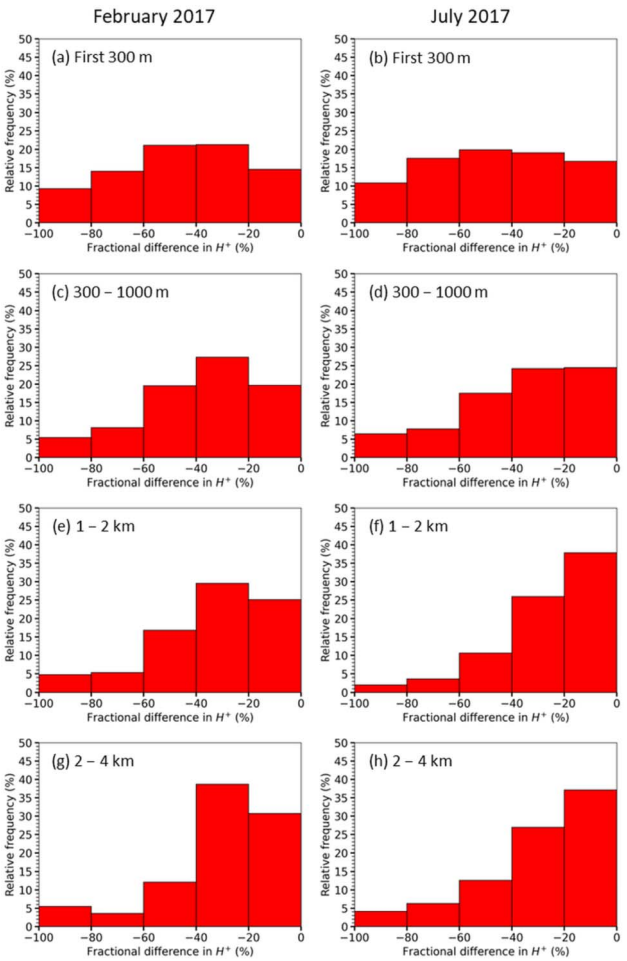

Fig. 5 Frequency distributions of the fractional difference in H^+ concentrations at 10 min intervals between large and small droplets over the US during February and July 2017 at different altitudes: (a) and (b) first 300 m, (c) and (d) 300–1000 m, (e) and (f) 1000–2000 m, (g) and (h) 2000–4000 m. A negative fractional difference indicates that large droplets are more alkaline than small droplets.

4.3 Bulk droplet approach

An additional simulation was performed for both months assuming that all droplets have the same size and composition (bulk approach). The average predicted bulk pH during February and July 2017 for different altitudes are shown in Fig. S13 and S14, respectively (SI). In most cases, the bulk pH of droplets falls between that of small and large droplets (Fig. S15–S16, SI). However, in some areas, such as North and South Dakota during winter, the pH of bulk droplets is even higher than that of large droplets. This occurs because in the bulk simulation, droplets can absorb gases (*e.g.*, NH_3) faster than the large droplets in the size-resolved simulation due to their higher surface area to volume ratio, while containing all the alkaline dust of the PM.

Previous studies[2,13,14] have shown that bulk aqueous phase models tend to predict lower sulfate production rates in the US compared to size-resolved models under many conditions. However, when there are small pH differences in droplets of different sizes bulk and size-resolved models produce similar

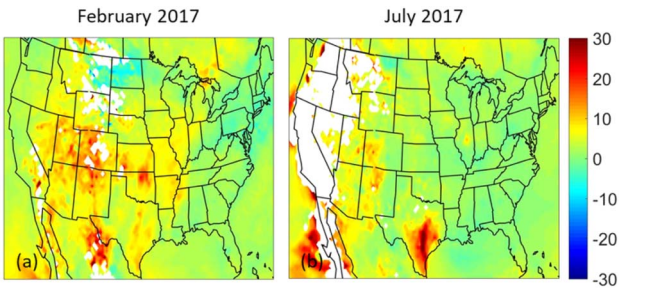

Fig. 6 Average percentage difference between the pH of large and small droplets at altitudes between 640 and 980 m during: (a) February 2017, and (b) July 2017. The white color corresponds to cloud and fog free areas. A positive fractional difference indicates that large droplets are more alkaline than small droplets.

predictions. Models such as the VSRM try to address these underestimations while saving computational time. In this work, we also investigated the impact of the bulk droplet assumption on aerosol composition. We compared the aqueous-phase sulfate production over the US with predictions from two-section size-resolved chemistry calculations. In general, the fractional difference in aqueous-phase sulfate concentrations over the US for 2017 between the two-section size-resolved and bulk chemistry calculations is relatively low and usually less than 20% at all altitudes for both simulated periods (Fig. S17, SI). Additionally, for hourly total PM_{10} sulfate, nitrate, and ammonium concentrations (Fig. S18–S20, SI), the fractional difference over the US between the two-section size-resolved and bulk chemistry calculations is low and usually less than 10%. Fahey and Pandis (2003)[14] showed that, on a daily basis, the percentage difference in aqueous-phase sulfate production between the VSRM and the bulk assumption in the South coast of California during 1995 could vary from 10% to 200%. They also found that the percentage of size-resolved aqueous-phase chemistry module calls was high in most areas ranging from 5% in areas with high NH_3 emissions to 100%. We also examined how often each approach is used in VSRM when the decision algorithm of Fahey and Pandis (2001)[13] is applied. During wintertime, the bulk droplet assumption is applied in approximately 96% of cases, while during summertime, increases to 99.6%.

All of the above suggest that bulk aqueous-phase chemistry calculations can simulate current aerosol composition across the US for 2017 conditions with small discrepancies mainly due to the significant decrease of acidic atmospheric pollutants levels (*e.g.*, SO_2 emissions) compared to 30 years ago. As a result, initial SO_2 concentrations are now often lower than those of H_2O_2, reducing the role of the pH-dependent ozone pathway, and leading the VSRM decision algorithm to favor the bulk approach. Please note that these conclusions apply to the US and not to regions with high SO_2 emissions.

According to the VSRM algorithm, SO_2 levels influence the decision between bulk and size-resolved simulation when the SO_2 concentration exceeds 12 ppb or when $H_2O_2 < 0.9\ SO_2$. To investigate this further, we examined this concentration difference (H_2O_2–$0.9\ SO_2$) in vertical layers with substantial cloud presence for both simulated periods (Fig. 7). During wintertime, the difference between H_2O_2 and SO_2 levels are low (up to 1 ppb) especially in the northern part of the US. On the contrary, during summer, this difference is higher (up to 4 ppb) due to the higher concentrations of H_2O_2 driven by the increased photochemical activity. SO_2 levels are lower than 0.5–1 ppb in most areas (Fig. S21, SI). These results indicate that a relatively small increase in SO_2 levels (of 0.5–1 ppb) during winter may be enough to influence the difference between the bulk and sectional approaches, while during summer higher increases are needed to have a similar impact.

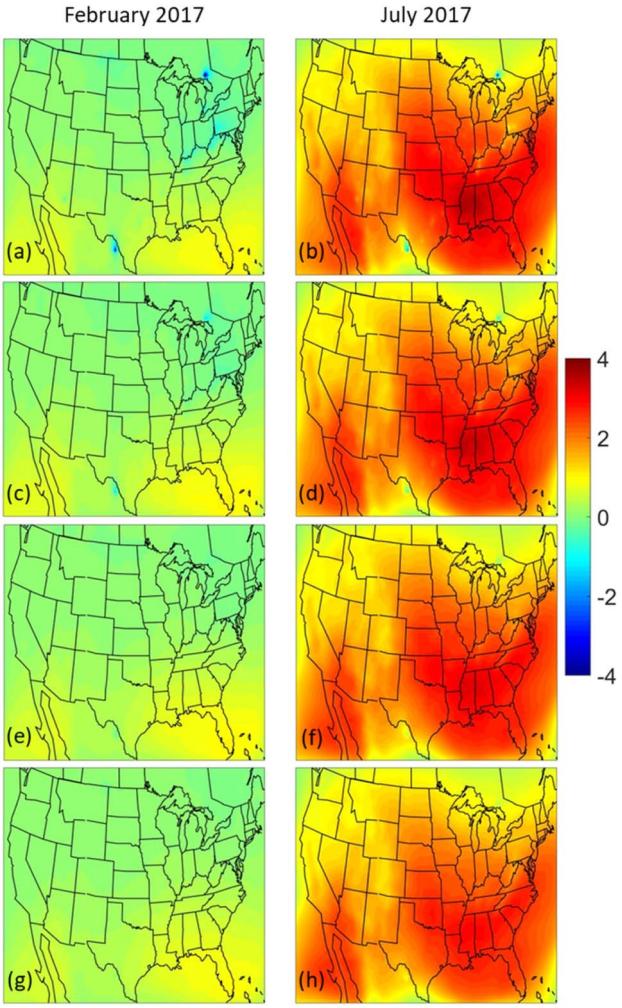

Fig. 7 Average difference between H_2O_2 and SO_2 concentrations (in ppb) as a function of altitude at: (a) and (b) 480–640 m, (c) and (d) 640–980 m, (e) and (f) 980–1340 m, (g) and (h) 1340–1720 m during February and July 2017. A positive difference indicates that H_2O_2 levels are higher.

4.4 Comparison with cloud pH measurements

There are numerous studies on cloud water pH in various regions of the US.[12,32–37] However, most were conducted over three decades ago. The reduction of SO_2 levels over the past 30 years resulted in significant changes in cloud droplet composition. For example, the chemical system at Whiteface Mountain has shifted away from being dominated by sulfate to one that is now mainly influenced by base cations.[38] Therefore, to evaluate our predictions, we compared the results with cloud water pH measurements from more recent studies (Fig. 8 and Table S1, SI). These comparisons are illustrative and not intended as a formal evaluation of the simulation outputs. We include some older measurements since there are no recent measurements in the particular region considering also that the sites are relatively remote and the droplet pH may have not changed significantly during the past few years.

Boris *et al.* (2018)[39] reported an average cloud water pH of 5.9 ± 0.4 at Casitas Pass in southern California during the summer of 2015. PMCAMx predicted a little higher value of 6.9 ± 0.6 during summer of 2017. Hutchings *et al.* (2009)[40] observed a mean cloud water pH of 6.3 ± 0.4 for Mt. Elden in Arizona

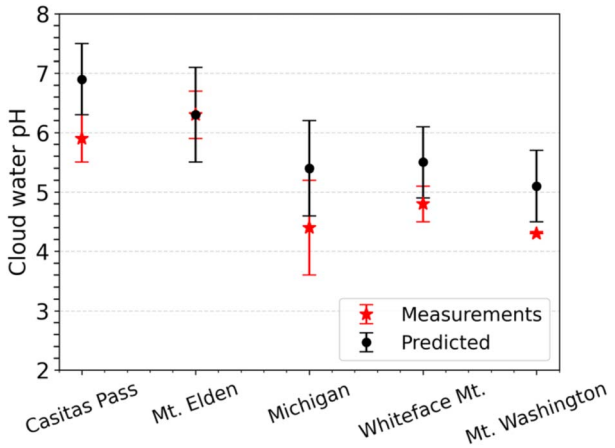

Fig. 8 Measured and predicted droplet pH at the examined sites. Values are presented as means ± standard deviations for both observations and predictions. Measurements were conducted during different summer periods, while predictions correspond to July 2017 simulation. Measured pH values refer to cloud water, whereas predicted values represent bulk droplet pH.

during the summers of 2005 and 2007, which is consistent with the PMCAMx predictions (6.3 ± 0.8). Hill *et al.* (2007)[41] reported an average cloud water pH of 4.4 ± 0.8 in Michigan during the summer of 2005. PMCAMx predicted a little higher bulk droplet pH value of 5.4 ± 0.8 during summer. At Whiteface Mountain, the average measured cloud water pH was 4.8 ± 0.3 during the summer of 2014.[42] PMCAMx predicted a bulk droplet pH value of 5.5 ± 0.6 during summer. Murray *et al.* (2013)[43] reported an average cloud water pH of 4.3 at Mt. Washington during the summers of 2008 and 2010. The bulk droplet pH prediction in this region equals to 5.1 ± 0.6 during summer.

Although small discrepancies exist between the measurements and PMCAMx predictions, these are likely due to small differences in temporal factors, such as variations in dust, NH_3 and SO_2 levels. Despite these minor differences, the model predictions are reasonable.

5. Conclusions

Size-resolved cloud and fog droplet acidity was simulated over the US during wintertime and summertime period. Higher droplet pH was predicted in the western part of the US for both simulated periods due to the higher dust concentrations for both droplet sizes. In contrast, the presence of higher concentrations of acidic particle components (*e.g.*, sulfate) and acidic gases that can dissolve in droplets water led to lower droplet pH predictions in the eastern US and in marine areas with variations influenced also by ammonia emissions during the two simulated periods. The decrease in concentration of particles and gases with altitude results in a corresponding change in droplets pH. In the western US, cloud pH is mainly influenced by higher dust concentrations, which decrease with altitude, leading in turn to lower droplet pH at higher altitudes. In contrast, in the eastern US, where acidic components are more dominant, their decrease with altitude leads to higher pH predictions at higher altitudes. Another factor influencing this change is the increase in cloud LWC with altitude.

Large droplets at all altitudes were more alkaline (up to 100% lower H^+ concentrations) than small especially in regions with higher dust concentrations during both simulated periods. However, the pH differences predicted by the two-section approach should be viewed as a lower limit of the actual pH droplet variation across the droplet size spectrum.[44] The bulk droplet assumption typically resulted in a droplet pH that was either close to or between the pH values of small and large droplets. The bulk droplet approach can simulate the current aerosol composition over the US with small discrepancies (less than 10% on average) compared to the two-section size-resolved chemistry calculations. Our simulations indicate that the current pH differences between small and large droplets in regions with high SO_2 emissions are lower than they were 30 years ago. Also, the current initial SO_2 concentrations are often lower than H_2O_2 concentrations across the US, leading the VSRM decision algorithm to favor the bulk droplet approach, given the small contribution of the pH-dependent ozone pathway to the aqueous-phase sulfate production. Please note that these conclusions are specific to the US and may not apply to regions with high SO_2 emissions. Our findings suggest that a small increase in SO_2 levels (approximately 0.5 ppb) during winter may be sufficient to influence the difference between the bulk and sectional approaches in the US. In contrast, during summer, higher SO_2 concentrations are required to produce a comparable effect.

Droplets acidity is an important property influencing a wide range of CTMs predictions, including atmospheric chemistry, PM formation, precipitation acidity, trace metal speciation and their response to emission changes. Our study suggests that the representation of droplet pH in CTMs does not significantly influence predictions across the US.

Author contributions

SK implemented dust effects on droplets composition and pH in VSRM, carried out the PMCAMx simulations and wrote the paper. GS introduced droplet pH as an output of PMCAMx. SNP conceived and led the study and helped in the writing of the paper.

Conflicts of interest

The authors declare that they have no conflicts of interest.

Data availability

All software programs used in this study are referenced throughout the Model description and Model application Sections of this work. Data files used to produce each figure are available in the Zenodo repository, accessible through the C-STACC community records, **https://zenodo.org/communities/c-stacc_group/records?q=&l=list&p=1&s=10&sort=newest**.

Supplementary information: Additional figures and information about the vertical distribution of simulated parameters. See DOI: https://doi.org/10.1039/d5ea00067j.

Acknowledgements

This work was supported by the European Union's Horizon Europe project "CleanCloud" (grant agreement no. 101137639).

References

1 A. Tilgner, P. Bräuer, R. Wolke and H. Herrmann, *J. Atmos. Chem.*, 2013, **70**, 221–256.
2 H. O. T. Pye, A. Nenes, B. Alexander, A. P. Ault, M. C. Barth, S. L. Clegg, J. L. Collett Jr, K. M. Fahey, C. J. Hennigan, H. Herrmann, M. Kanakidou, J. T. Kelly, I.-T. Ku, V. F. McNeill, N. Riemer, T. Schaefer, G. Shi, A. Tilgner, J. T. Walker, T. Wang, R. Weber, J. Xing, R. A. Zaveri and A. Zuend, *Atmos. Chem. Phys.*, 2020, **20**, 4809–4888.
3 A. Tilgner, T. Schaefer, B. Alexander, M. Barth, J. L. Collett Jr, K. M. Fahey, A. Nenes, H. O. T. Pye, H. Herrmann and V. F. McNeill, *Atmos. Chem. Phys.*, 2021, **21**, 13483–13536.
4 J. H. Seinfeld and S. N. Pandis, *Atmospheric Chemistry and Physics. From Air Pollution to Climate Change.* 3rd edn, Wiley, New Jersey, 2016.
5 X. Liu, R. C. Easter, S. J. Ghan, R. Zaveri, P. Rasch, X. Shi, J.-F. Lamarque, A. Gettelman, H. Morrison, F. Vitt, A. Conley, S. Park, R. Neale, C. Hannay, A. M. L. Ekman, P. Hess, N. Mahowald, W. Collins, M. J. Iacono, C. S. Bretherton, M. G. Flanner and D. Mitchell, *Geosci. Model Dev.*, 2012, **5**, 709–739.
6 S. Myriokefalitakis, K. Tsigaridis, N. Mihalopoulos, J. Sciare, A. Nenes, K. Kawamura, A. Segers and M. Kanakidou, *Atmos. Chem. Phys.*, 2011, **11**, 5761–5782.
7 B. Alexander, D. J. Allman, H. M. Amos, T. D. Fairlie, J. Dachs, D. A. Hegg and R. S. Sletten, *J. Geophys. Res.:Atmos.*, 2012, **117**, D06304.
8 J.-F. Lamarque, L. K. Emmons, P. G. Hess, D. E. Kinnison, S. Tilmes, F. Vitt, C. L. Heald, E. A. Holland, P. H. Lauritzen, J. Neu, J. J. Orlando, P. J. Rasch and G. K. Tyndall, *Geosci. Model Dev.*, 2012, **5**, 369–411.
9 D. Simpson, A. Benedictow, H. Berge, R. Bergström, L. D. Emberson, H. Fagerli, C. R. Flechard, G. D. Hayman, M. Gauss, J. E. Jonson, M. E. Jenkin, A. Nyíri, C. Richter, V. S. Semeena, S. Tsyro, J.-P. Tuovinen, Á. Valdebenito and P. Wind, *Atmos. Chem. Phys.*, 2012, **12**, 7825–7865.
10 S. Watanabe, T. Hajima, K. Sudo, T. Nagashima, T. Takemura, H. Okajima, T. Nozawa, H. Kawase, M. Abe, T. Yokohata, T. Ise, H. Sato, E. Kato, K. Takata, S. Emori and M. Kawamiya, *Geosci. Model Dev.*, 2011, **4**, 845–872.
11 O. A. Søvde, M. J. Prather, I. S. A. Isaksen, T. K. Berntsen, F. Stordal, X. Zhu, C. D. Holmes and J. Hsu, *Geosci. Model Dev.*, 2012, **5**, 1441–1469.
12 J. L. Collett, A. Bator, X. Rao and B. B. Demoz, *Geophys. Res. Lett.*, 1994, **21**, 2393–2396.
13 K. M. Fahey and S. N. Pandis, *Atmos. Environ.*, 2001, **35**, 4471–4478.
14 K. M. Fahey and S. N. Pandis, *J. Geophys. Res.*, 2003, **108**, 4690–4701.
15 J. Hu, Y. Yin and Q. Chen, *J. Geophys. Res.:Atmos.*, 2019, **124**, 424–440.
16 V. Shah, D. J. Jacob, J. M. Moch, X. Wang and S. Zhai, *Atmos. Chem. Phys.*, 2020, **20**, 12223–12245.
17 Environ, *User's Guide to the Comprehensive Air Quality Model with Extensions (CAMx), Version 6.00*, Novato, CA, 2013, available at: https://www.camx.com/Files/CAMxUsersGuide_v6.00.pdf, accessed 28 May 2025.
18 W. P. L. Carter, *Documentation of the SAPRC-99 Chemical Mechanism for VOC Reactivity Assessment*, Report to California Air Resources Board, 2000, available at: https://intra.engr.ucr.edu/~carter/reactdat.htm, accessed 28 May 2025.
19 S. Kakavas, S. N. Pandis and A. Nenes, *Tellus B*, 2022, **74**, 1–23.
20 K. M. Cerully, A. Bougiatioti, J. R. Hite Jr, H. Guo, L. Xu, N. L. Ng, R. Weber and A. Nenes, *Atmos. Chem. Phys.*, 2015, **15**, 8679–8694.
21 N. M. Donahue, A. L. Robinson, C. O. Stanier and S. N. Pandis, *Environ. Sci. Technol.*, 2006, **40**, 2635–2643.
22 S. N. Pandis and J. H. Seinfeld, *J. Geophys. Res.*, 1989, **94**, 1105–1126.
23 M. D. Petters and S. M. Kreidenweis, *Atmos. Chem. Phys.*, 2007, **7**, 1961–1971.
24 A. Bougiatioti, A. Nenes, J. J. Lin, C. A. Brock, J. A. de Gouw, J. Liao, A. M. Middlebrook and A. Welti, *Atmos. Chem. Phys.*, 2020, **20**, 12163–12176.
25 A. Eyth and J. Vukovich, *Technical Support Document (TSD): Preparation of Emissions Inventories for the Version 6.3, 2011 Emissions Modeling Platform*, US Environmental Protection Agency, Office of Air Quality Planning and Standards, 2016.
26 V. A. Karydis, A. P. Tsimpidi, A. Pozzer, M. Astitha and J. Lelieveld, *Atmos. Chem. Phys.*, 2016, **16**, 1491–1509.
27 M. Liaskoni, P. Huszar, L. Bartík, A. P. Prieto Perez, J. Karlický and O. Vlček, *Atmos. Chem. Phys.*, 2023, **23**, 3629–3654.
28 S. Kakavas, E. Siouti, A. Nenes and S. N. Pandis, *Atmos. Environ.*, 2025, **345**, 121056.
29 R. E. Morris, D. E. McNally, T. W. Tesche, G. Tonnesen, J. W. Boylan and P. Brewer, *J. Air Waste Manage. Assoc.*, 2005, **55**, 1694–1708.
30 A. Bator and J. L. Collett, *J. Geophys. Res.*, 1997, **102**, 28071–28078.
31 J. Collett, R. Iovinelli and B. Demoz, *Atmos. Environ.*, 1995, **29**, 1145–1154.
32 J. W. Munger, J. Collett Jr, B. Daube Jr and M. R. Hoffmann, *Atmos. Environ.*, 1990, **24**, 185–205.
33 D. S. Kim and V. P. Aneja, *Tellus B*, 1992, **44**, 41–53.
34 Y. Erel, S. O. Pehkonen and M. R. Hoffmann, *J. Geophys. Res.*, 1993, **98**, 18423–18434.
35 X. Rao and J. L. J. Collett, *Environ. Sci. Technol.*, 1995, **29**, 1023–1031.
36 R. L. Siefert, A. M. Johansen, M. R. Hoffmann and S. O. Pehkonen, *J. Air Waste Manage. Assoc.*, 1998, **48**, 128–143.

37 J. L. Collett Jr, K. J. Hoag, X. Rao and S. N. Pandis, *Atmos. Environ.*, 1999, **33**, 4833–4847.
38 C. E. Lawrence, P. Casson, R. Brandt, J. J. Schwab, J. E. Dukett, P. Snyder, E. Yerger, D. Kelting, T. C. VandenBoer and S. Lance, *Atmos. Chem. Phys.*, 2023, **23**, 1619–1639.
39 A. J. Boris, D. C. Napolitano, P. Herckes, A. L. Clements and J. L. Collett Jr, *Aerosol Air Qual. Res.*, 2018, **18**, 224–239.
40 J. W. Hutchings, M. S. Robinson, H. McIlwraith, J. Triplett Kingston and P. Herckes, *Water, Air, Soil Pollut.*, 2009, **199**, 191–202.
41 K. A. Hill, P. B. Shepson, E. S. Galbavy, C. Anastasio, P. S. Kourtev, A. Konopka and B. H. Stirm, *J. Geophys. Res.*, 2007, **112**, D11301.
42 R. D. Cook, Y.-H. Lin, Z. Peng, E. Boone, R. K. Chu, J. E. Dukett, M. J. Gunsch, W. Zhang, N. Tolic and A. Laskin, *Atmos. Chem. Phys.*, 2017, **17**, 15167–15180.
43 G. L. D. Murray, K. D. Kimball, L. B. Hill, J. E. Hislop and K. C. Weathers, *Water, Air, Soil Pollut.*, 2013, **224**, 1653.
44 K. F. Moore, D. E. Sherman, J. E. Reilly and J. L. Collett Jr, *Atmos. Environ.*, 2004, **38**, 1389–1402.